THE ASTROPHYSICAL JOURNAL, 420:445–449, 1994 January 10

COSMIC MICROWAVE BACKGROUND DIPOLE SPECTRUM MEASURED BY THE *COBE*[1] FIRAS INSTRUMENT

D. J. FIXSEN,[2] E. S. CHENG,[3] D. A. COTTINGHAM,[4] R. E. EPLEE, JR.,[5] R. B. ISAACMAN,[5] J. C. MATHER,[3]
S. S. MEYER,[6] P. D. NOERDLINGER,[2] R. A. SHAFER,[3] R. WEISS,[6] E. L. WRIGHT,[7] C. L. BENNETT,[3]
N. W. BOGGESS,[3] T. KELSALL,[3] S. H. MOSELEY,[3] R. F. SILVERBERG,[3]
G. F. SMOOT,[8] AND D. T. WILKINSON[9]
Received 1993 February 5; accepted 1993 July 21

ABSTRACT

The FIRAS instrument on the *COBE* has determined the dipole spectrum of the cosmic microwave background radiation (CMBR) from 2 to 20 cm^{-1}. For each frequency the signal is decomposed by fitting to a monopole, a dipole, and a Galactic template for $\sim 60\%$ of the sky. The overall dipole spectrum fits the derivative of a Planck function with an amplitude of 3.343 ± 0.016 mK (95% confidence level), a temperature of 2.714 ± 0.022 K (95% confidence level), and an rms deviation of 6×10^{-9} ergs cm^{-2} s^{-1} sr^{-1} cm limited by detector and cosmic-ray noise. The monopole temperature is consistent with that determined by direct measurement in the accompanying article by Mather et al.

Subject headings: cosmic microwave background — cosmology: observations — early universe

1. INTRODUCTION

We report the high-frequency determination (>90 GHz) of the detailed spectrum of the cosmic microwave background radiation (CMBR) dipole, measured by the FIRAS (Far-Infrared Absolute Spectrophotometer) on the *COBE* (*Cosmic Background Explorer*) satellite. The dipole term is generally interpreted as a Doppler shift due to the Earth's motion. The apparent background temperature for an observer moving with velocity v with respect to the rest frame of the blackbody radiation is (Peebles & Wilkinson 1968)

$$T_{\rm obs} = T_{\rm cmbr} \frac{\sqrt{1-(v/c)^2}}{1-(v/c)\cos\theta} \approx T_{\rm cmbr}[1+(v/c)\cos\theta] , \quad (1)$$

where θ is the angle between the line of sight and the direction of the motion of the observer. The second-order term in v/c is a quadrupole with amplitude ~ 2 μK, which is much smaller than the cosmic quadrupole measured by the *COBE* DMR (Differential Microwave Radiometer) (Smoot et al. 1992). The observer's motion is the vector sum of many terms: the orbital motions of the Earth around the Sun, the Sun around the Galaxy, and the peculiar velocity of the Galaxy with respect to the reference frame of the universe.

Equation (1) implies an explicit prediction of the spectrum of the dipole: the observed spectrum as a function of θ must be

$$S_\nu(\theta) = B_\nu(T_{\rm obs}) \approx B_\nu(T_{\rm cmbr}) + \left(\frac{v}{c}\right) T_{\rm cmbr} \left.\frac{\partial B_\nu}{dT}\right|_{T_{\rm cmbr}} \cos\theta , \quad (2)$$

where $B_\nu(T)$ is the Planck function. This equation shows that the dipole part of the spectrum must have the shape of the derivative of the Planck function with respect to temperature, evaluated at the temperature of the CMBR. This test has been done in the past by measuring the amplitude of the dipole at discrete frequencies up to 90 GHz. Measurements of the dipole in this frequency range reported by Fixsen, Cheng, & Wilkinson (1983); Lubin et al. (1985); Klypin et al. (1987); Cottingham (1987); and Smoot et al. (1992) are all in agreement on both the amplitude and the direction.

Many other astrophysical sources are asymmetrically distributed in the sky and thereby could contribute to a dipole anisotropy. Possible sources include the following. The dust associated with the solar system is anisotropic, and it has long been noted that the principal axis of the microwave dipole lies close to the ecliptic plane ($\sim 11°$). There is a large dipole component in the distribution of Galactic sources, due to our position far from the Galactic center. The *IRAS* galaxy counts show a dipole anisotropy (Scharf et al. 1992). The X-ray background also shows a dipole anisotropy (Miyaji & Bolt 1990; Shafer 1983), indicating that infrared emission from these sources might also contribute. However, in each case it is difficult to imagine a plausible emission mechanism that would produce a spectrum that would closely resemble the derivative of a Planck function at the temperature of the CMBR on both the Rayleigh-Jeans and Wien sides of the curve. Thus an accurate measurement of the spectrum of the dipole over a range of frequencies spanning the peak of the curve provides a strong test of whether it is due to a Doppler shift of the CMBR.

2. INSTRUMENT DESCRIPTION AND DATA ANALYSIS

The FIRAS is a polarizing Michelson interferometer. This instrument is described briefly by Mather et al. (1990). It mea-

[1] The National Aeronautics and Space Administration/Goddard Space Flight Center (NASA/GSFC) is responsible for the design, development, and operation of the *Cosmic Background Explorer* (*COBE*). Scientific guidance is provided by the *COBE* Science Working Group. GSFC is also responsible for the development of the analysis software and for the production of the mission data sets.

[2] Applied Research Corporation, Code 685.3, NASA/GSFC, Greenbelt, MD 20771.
[3] NASA Goddard Space Flight Center, Code 685, Greenbelt, MD 20771.
[4] Universities Space Research Association, Code 685.3, NASA/GSFC, Greenbelt, MD 20771.
[5] General Sciences Corporation, Code 685.3, NASA/GSFC, Greenbelt, MD 20771.
[6] MIT Department of Physics, Room 20F-001, Cambridge, MA 02139.
[7] UCLA Astronomy Department, Los Angeles, CA 90024-1562.
[8] LBL and SSL, University of California, Berkeley, CA 94720.
[9] Princeton University Physics Department, Princeton, NJ 08540.

sures the spectral difference between a 7° patch of sky and an internal blackbody. An external blackbody calibrator is intermittently placed in the input aperture to provide an absolute calibration signal. The interferometer covers the frequency range from 2 to 95 cm^{-1} in two bands separated at 20 cm^{-1}. It has two output ports (left and right), each split into these two spectral bands (high and low), so there are a total of four detectors. There are two scan lengths (short and long) and two scan speeds (slow and fast) for a total of four scan modes. The results reported here are based on one detector and one scan mode ("left low short slow"). In the short scan modes the instrument has a spectral resolution of 0.7 cm^{-1}.

The data are received as 512 point interferograms, accompanied by engineering data giving relevant temperatures, voltages, currents, and spacecraft orientation. These interferograms are sorted into groups by sky position and instrument state. The groups are checked, compared, deglitched, averaged, and Fourier-transformed. The data taken with the external calibrator in the input aperture were used to construct a calibration model for each detector/scan mode combination. The calibration models are then used to calibrate the sky data as described by Fixsen et al. (1994). The result is a calibrated sky map for each detector and scan mode.

Each averaged spectrum is accompanied by a noise spectrum derived from the self-consistency of the individual interferograms, used as a basis for the χ^2 computations throughout. For the low-frequency data reported in this paper, there are 34 spectrum points spaced equally from 2 to 21 cm^{-1}. The spectra are adjusted to the solar system barycenter to account for the Earth's orbital velocity around the Sun, which would otherwise be readily detectable as an additional variable dipole of amplitude 0.3 mK. For this paper, we use data taken throughout the 10 month observing lifetime of the FIRAS.

The FIRAS points at the zenith as the *COBE* orbits the Earth with a period of 103 minutes. The orbit plane is maintained approximately perpendicular to the direction to the Sun. This scan pattern concentrates the observing time near the ecliptic poles. We divide the sky into 6144 equal area pixels according to the quadrilateralized spherical cube representation (O'Neill & Laubscher 1976). The "left low short slow" data set used here has data for 5308 of the 6144 pixels.

The data are separately fitted at each frequency to a model consisting of three spatial components. The first component is a uniform distribution over the sky, the spatial model of the CMBR. The second component is cos θ, where θ is the angle from the hot pole of the dipole, $(\alpha, \delta) = (168.^{\circ}3 \pm 0.^{\circ}5, -7.^{\circ}2 \pm 0.^{\circ}5)$ (Smoot et al. 1992). (Throughout this paper equatorial coordinates refer to the equator and equinox of J2000.0.) The third component, the spatial distribution of the total power received in the high-frequency FIRAS channel above 25 cm^{-1}, is used as a template for the Galaxy spectrum under the assumption that the high-frequency ($25 < \nu < 80$ cm^{-1}) radiation is well correlated to the low-frequency ($2 < \nu < 20$ cm^{-1}) Galactic radiation. The high-frequency channel is centered on 41 cm^{-1} with a 44 cm^{-1} effective bandwidth. Since the high- and low-frequency data are taken simultaneously through the same horn there is little mismatch in sky coverage and no need for beam convolution. Alternatively, we take the third component to be csc $|b|$, where b is Galactic latitude. This is clearly an oversimplification of the Galaxy, but our results are independent of the Galactic model used. This provides strong evidence that our results are not contaminated by any inadequacy of the high-frequency FIRAS power distribution as a model of the low-frequency Galactic emission. Except where noted otherwise, the results reported here are based on the FIRAS high-frequency Galactic model.

The Galaxy shows clear features in spectrum and position so the region $|b| < 20°$ was excluded in the fits. This selection differs from Mather et al. (1994); here we preserve the inherent rejection of certain systematic effects (time-dependent offsets and potential Galactic effects) by maintaining symmetry of the sky coverage. For any point which is deleted, the symmetric point, or opposite point, is also deleted. As the dipole is antisymmetric on the sky, it produces a signal on the detector which is antisymmetric on each orbit; thus the dipole signal is effectively chopped at the orbital period of 103 minutes. The stability of the instrument is such that there are no significant systematic effects that fluctuate at or above this frequency, and therefore only the detector noise is significant for the dipole spectrum.

The data are weighted by the integration time, or number of interferograms, as there are no significant variations in detector noise for all-sky data. The parameters which are determined from the fit are the linear coefficients of the three spatial components discussed above, done independently at each frequency. Thus the result can be viewed as three spectra, one for each spatial component. It is important to note that this fit makes no a priori assumptions about the forms of these spectra; only their spatial distribution is posited. Let N be the number of pixels used in a fit, where $N = 3517$. S is the $N \times 34$ matrix of data and V is the $3 \times N$ matrix, where the three rows are the spatial forms of the three components, and each element is the value of the template at that pixel (the uniform model is 1 everywhere). W is the diagonal weight matrix, the number of interferograms at each pixel. The best-fit spectra associated with the three spatial components are contained in the fit solution matrix M, which is computed by

$$M = (VWV^T)^{-1}VWS\,. \tag{3}$$

The resulting uniform, dipole, and Galactic spectra are displayed in Figure 1. This procedure also produces a variance matrix $\sigma^2(VWV^T)^{-1}$, where σ^2 is the uncertainty of a spectrum made from a single interferogram. The diagonal elements of the covariance matrix are the estimate of the uncertainty in each spectrum, which includes the uncertainty of the separation into these components. (The uncertainties are correlated but as we treat each spectrum individually we ignore this fact.)

3. RESULTS AND INTERPRETATION

The uniform spectrum derived here fits a blackbody spectrum of 2.726 ± 0.010 K (95% CL systematic; CL = confidence level); this spectrum (derived in a slightly different way) is discussed by Mather et al. (1994). The Galactic spectrum is adequately fitted by functions of the form $\nu^n B_\nu(T_{dust})$. Wright et al. (1991) examined the FIRAS Galaxy spectrum and found that it was fitted by $n = 1.65$ and $T_{dust} = 23.3$ K. The Galactic spectrum derived here, which is based only on data out of the Galactic plane, produces a slightly lower temperature, $T_{dust} = 20 \pm 1$ K, with n fixed at 1.5. This low-frequency spectrum does not have adequate signal-to-noise ratio to make an interesting simultaneous determination of both n and T_{dust}; a full discussion of the Galaxy requires the high-frequency data and will be dealt with in a later paper. Here the Galactic radiation is treated as a contaminant of the CMBR.

We fit the dipole spectrum to the derivative of a Planck function $T_{amp}\, dB_\nu(T_{cmbr})/dT$, where we fix $T_{cmbr} = 2.726$ K

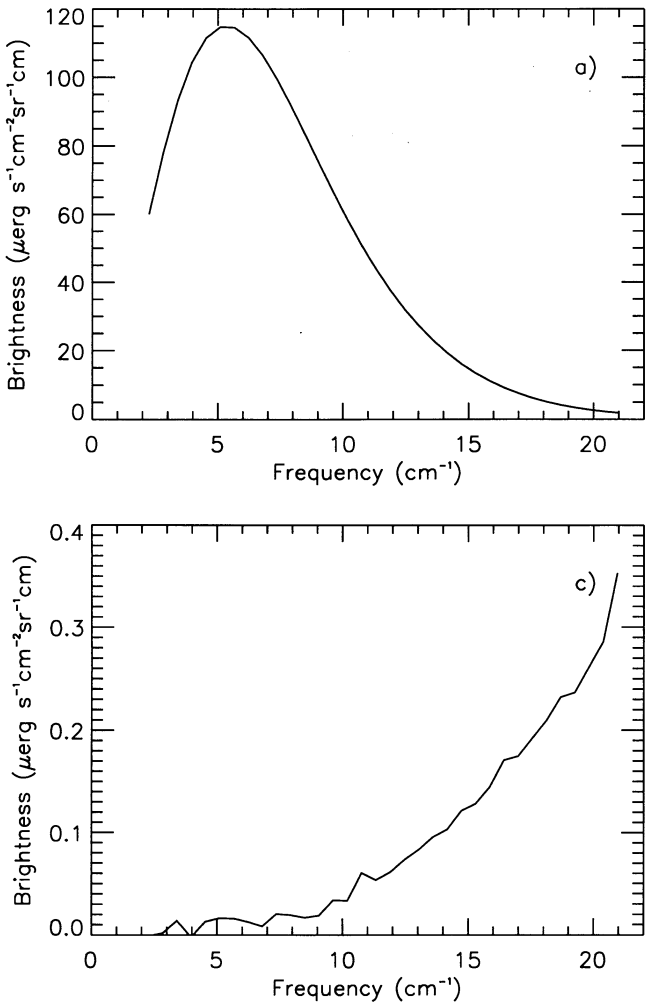

FIG. 1.—Best-fit spectra for each of the model components: (*a*) uniform; (*b*) dipole; (*c*) Galaxy.

(Mather et al. 1994) and allow T_{amp} to vary. The best-fit value of the dipole amplitude is $T_{amp} = 3.343 \pm 0.006$ mK; however, the result is dependent on the Galactic cut in a non-Gaussian fashion. We add in quadrature $\frac{1}{2}$ of the change in the result when the Galactic cut is changed from 10° to 40° as an estimate of the uncertainty in the final result to obtain: $T_{amp} = 3.343 \pm 0.016$ mK (95% CL). This is a reasonable approximation if the systematic Galactic effects are random numbers drawn from a uniform distribution having the measured width and thus an rms deviation of the range/$(12)^{1/2}$; we elect to be conservative by dividing by 2 instead, and note that although this is not a true 95% confidence limit, it is a useful summary of the confidence range. This result is summarized in Table 1.

TABLE 1

ERRORS AND DEPENDENCE ON GALACTIC CUT ANGLE[a]

Parameter	Value (unit)	σ	Galactic Range	95% CL
T_{amp}	3.343 mK	0.006	3.318–3.348	0.016
α	168°.9	0.15	168.5–169.2	0.5
δ	−7°.5	0.15	−7.5–−7.2	0.5
T_{cmbr}	2.714 K	0.006	2.701–2.727	0.022

[a] Galactic cut angle was varied from 10° to 40°.

Figure 2 shows the spectrum of the dipole derived using either Galactic spatial model, and the best-fit differential Planck spectrum.

The differences between the dipole spectrum and the fitted Planck derivative are shown in Figure 3 and in Table 2. The deviations from the blackbody derivative dipole spectrum are only 6×10^{-9} ergs cm^{-2} s^{-1} sr^{-1} cm rms, a factor of 5 smaller than the difference between the monopole and its fitted blackbody. These deviations are 1% of the maximum dipole signal, 4.8×10^{-7} ergs cm^{-2} s^{-1} sr^{-1} cm at 7.25 cm^{-1}.

To find the dipole direction, we first fit, by χ^2 minimization, two free parameters, a CMBR temperature and a Galactic dust optical depth, at each pixel. The CMBR temperature assumes a Planck spectrum and the dust spectrum is of the form $\nu^{1.5}B_\nu(20\ \mathrm{K})$. This spectrum was chosen as it matches the shape of the spectrum in the Galactic plane. This yields maps of the CMBR temperature and the dust optical depth. Next, a monopole plus three dipole components are fitted to the temperature map.

The vector sum of the dipole coefficients points in the

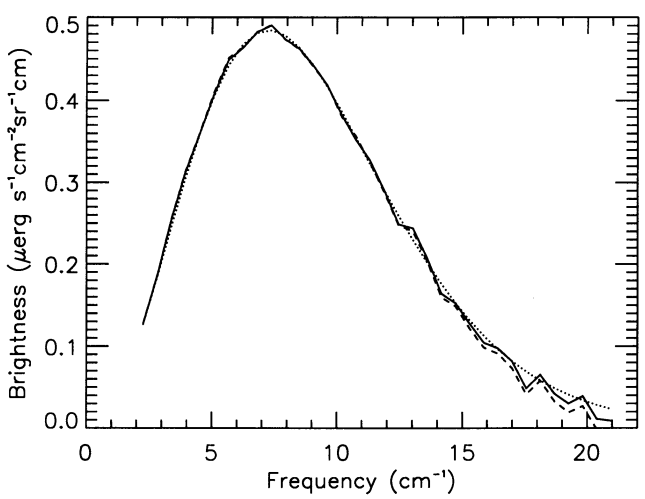

FIG. 2.—Dipole spectrum. *Solid line*, using FIRAS high-frequency Galactic spatial model; *dashed line*, using csc |*b*| Galactic spatial model; *dotted line*, best-fit of derivative of Planck function to solid line.

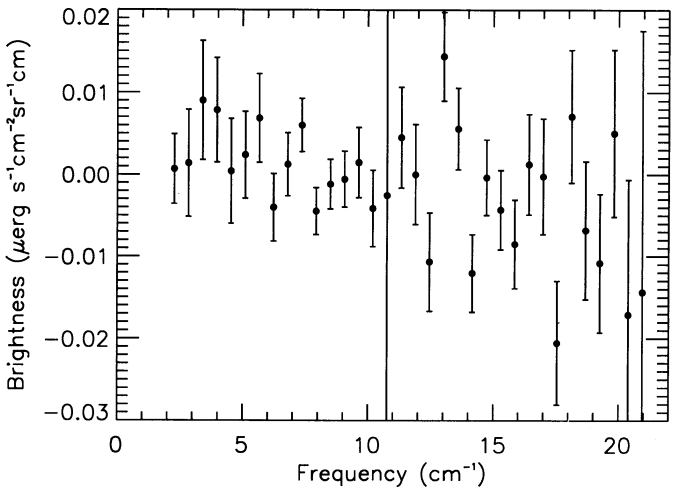

FIG. 3.—Residual of dipole spectrum from best-fit derivative of Planck function.

direction $(\alpha, \delta) = (168.^{\circ}9 \pm 0.^{\circ}5, -7.^{\circ}5 \pm 0.^{\circ}5)$, or $(b, l) = (48.^{\circ}3, 265.^{\circ}6)$, consistent with the direction from the DMR results. Again data for $|b| < 20^{\circ}$ were excluded from the fit because of the potential inaccuracy of the model of the Galaxy.

The amplitude of the dipole is in agreement with that measured by the *COBE* DMR (Smoot et al. 1992), $T_{amp} = 3.36 \pm 0.10$ mK, derived from observations at 31.5 GHz, 53 GHz, and 90 GHz. Previous dipole amplitude determinations extending to frequencies above 3 cm^{-1} or 90 GHz include Fabbri et al. (1980) and Halpern et al. (1988) who report $T_{amp} = 2.9^{+1.3}_{-0.6}$ mK, in the direction $(\alpha, \delta) = (170^{\circ} \pm 10^{\circ}, 3^{\circ} \pm 10^{\circ})$ and $T_{amp} = 3.4 \pm 0.4$ mK, in the direction $(\alpha, \delta) = (182^{\circ} \pm 4^{\circ}, -23^{\circ} \pm 5^{\circ})$, respectively. The amplitudes are in agreement, though the directions are inconsistent with that measured by the DMR. More recently Ganga et al. (1993) have measured a dipole direction $(\alpha, \delta) = (169.^{\circ}1 \pm 0.^{\circ}5, -7.^{\circ}4 \pm 0.^{\circ}5)$ at 6 cm^{-1}, consistent with the DMR measurement; they do not report an amplitude, as they use it as their calibration.

By choosing the monopole temperature as the point to evaluate dB_ν/dT, we have forced the dipole temperature to be that of the monopole. If we fit both T_{amp} and T_{cmbr}, we obtain $T_{cmbr} = 2.714 \pm 0.006$ K (1 σ statistical error), which reduces the χ^2 from 47 for 33 DOF (degrees of freedom) to 43.3 for 32 DOF. However, there is a systematic dependence on the Galactic latitude cut; as the cut is changed from 15° to 40° the fitted temperature changes from 2.701 to 2.727 K. We add $\frac{1}{3}$ of the range of the fitted temperature to estimate the uncertainty from systematic Galaxy component to get 2.714 ± 0.022 K (95% CL). The agreement of the dipole temperature with the monopole temperature is consistent with the conventional Doppler interpretation of the dipole. It is also a confirmation that the overall temperature scale and calibration adjustments for the FIRAS are consistent.

The implication for cosmology is clear: the dipole is a part of the CMBR and is probably caused by the Doppler shift from the Earth's peculiar velocity relative to the comoving frame, and in small part (~1%) by the dipole component of the Harrison-Zel'dovich-Peebles anisotropy spectrum. It would require an extraordinary coincidence for this spectrum to be produced by anything other than the same surface that emitted the CMBR, and therefore it is no longer plausible to speculate that the dipole is the result of local emission sources in the ecliptic plane, the Galaxy, other galaxies, or the intergalactic medium. The close alignment of the dipole with the ecliptic plane must now be viewed as only a coincidence. There does exist a reference frame in which the CMBR is a nearly isotropic blackbody.

4. SUMMARY

The CMBR has a dipole spectrum consistent with its thermal origin and a Doppler shift. The dipole itself has a differential thermal spectrum the temperature of which, 2.714 ± 0.022 K (95% CL), agrees with the monopole temperature (2.726 ± 0.010 K [95% CL systematic]). The rms deviations from the thermal model of the dipole spectrum are 6×10^{-9} ergs cm^{-2} s^{-1} sr^{-1} cm, a part in 10^4 of the monopole spectrum peak and only 1% of the peak of the dipole spectrum. The dipole direction and amplitude are $(\alpha, \delta) = (168.^{\circ}9 \pm 0.^{\circ}5, -7.^{\circ}5 \pm 0.^{\circ}5)$ and 3.343 ± 0.016 mK (95% CL), in agreement with the microwave results from the DMR. The high-latitude Galactic emission is adequately described by a $\csc |b|$ form with a fixed spectrum, and the Galactic spectrum is consistent with dust with an emissivity index of $n = 1.5$ and temperature 20 K.

TABLE 2

RESIDUAL OF FIT AND UNCERTAINTIES

Frequency[a]	Residual[b]	Error[b]
2.27	0.7	4.3
2.83	1.4	6.5
3.40	9.0	7.2
3.96	7.8	6.4
4.53	0.4	6.4
5.10	2.4	5.3
5.66	6.9	5.4
6.23	−4.0	4.1
6.80	1.2	3.9
7.36	6.0	3.2
7.93	−4.5	2.9
8.50	−1.2	3.0
9.06	−0.6	3.4
9.63	1.5	4.3
10.19	−4.1	4.7
10.76	−2.5	66.0
11.33	4.5	6.1
11.89	0.0	6.1
12.46	−10.7	6.0
13.03	14.4	5.4
13.59	5.6	5.0
14.16	−12.0	4.7
14.72	−0.4	4.6
15.29	−4.3	4.9
15.86	−8.5	5.4
16.42	1.2	6.2
16.99	−0.2	7.1
17.56	−20.5	7.5
18.12	7.1	8.1
18.69	−6.8	8.4
19.26	−10.8	8.4
19.82	5.0	10.2
20.39	−17.1	16.5
20.95	−14.4	31.9

NOTE.—Residual of dipole spectrum from best-fit differential Planck spectrum. Errors include detector noise and effects of separating the dipole component from the other components.

[a] In cm^{-1}.

[b] In units of 10^{-9} ergs cm^{-2} s^{-1} sr^{-1} cm.

We thank our colleagues on the software and analysis team for the FIRAS, including S. Alexander, J. Gales, N. Gonzales, T. Hewagama, K. Jensen, S. Macwan, D. Massa, S. Read, L. Rosen, F. Shuman, A. Trenholme, and H. Wang. We also thank the engineering and flight operations staffs of NASA/GSFC for their support of this project. We would like to thank K. Jahoda and L. Page for useful discussions. Every achievement of the space program represents the creative and dedicated effort of many individuals, and no one person can possibly know of all the difficult problems that these people have solved.

REFERENCES

Cottingham, D. A. 1987, Ph.D. thesis, Princeton Univ
Fabbri, R., Guidi, I., Melchiorri, F., & Natale, V. 1980, Phys. Rev. Lett., 44, 23, 1563
Fixsen, D. J., Cheng, E. S., & Wilkinson, D. T. 1983, Phys. Rev. Lett., 50, 620
Fixsen, D. J., et al. 1994, 420, 457
Ganga, K. M., Cheng, E. S., Meyer, S. S., & Page, L. A. 1993, in preparation
Halpern, M., Benford, R., Meyer, S., Muehlner, D., & Weiss, R. 1988, ApJ, 332, 596
Klypin, A. A., Sazhin, M. V., Strukov, I. A., & Skulachev, D. P. 1987, Soviet Astron. Lett., 13, 104
Lubin, P. M., Villela, T., Epstein, G. L., & Smoot, G. F. 1985, ApJ, 298, L1
Mather, J. C., et al. 1990, ApJ, 354, L37
Mather, J. C., et al. 1994, ApJ, 420, 439
Miyaji, T., & Boldt, E. 1990, ApJ, 353, L3
O'Neill, E. M., & Laubscher, R. E. 1976, Extended Studies of a Quadrilateralized Spherical Cube Earth Data Base (NEPRF Tech. Rep. 3-76) (NTIS Rep. AD-A026294) (Computer Sciences Corp. CSC/TR-76/6008)
Peebles, P. J. E., & Wilkinson, D. T. 1968, Phys. Rev., 174, 2168
Scharf, C., Hoffman, Y., Lahav, O., & Lynden-Bell, D. 1992, MNRAS, 256, 229
Shafer, R. A. 1983, Ph.D. thesis, Univ. Maryland
Smoot, G. F., et al. 1992, ApJ, 396, L1
Wright, E. L., et al. 1991, ApJ, 381, 200